



1 **Air pollution reductions caused by the COVID-19 lockdown open up a way to preserve**
2 **the Himalayan snow cover**

3
4 Suvarna Fadnavis^{1*}, Bernd Heinold², Thazhe Purayil Sabin¹, Anne Kubin², Wan Ting Katty
5 Huang³, **Alexandru Rap⁴**, and **Rolf Müller⁵**

6 ¹Indian Institute of Tropical Meteorology, Centre for climate change research, Ministry of
7 Earth Sciences, India

8 ²Leibniz-Institut für Troposphärenforschung, Leipzig, Germany,

9 ³Department of Civil, Environmental and Geomatic Engineering, University College London,
10 London, United Kingdom

11 ⁴School of Earth and Environment, University of Leeds, Leeds, UK,

12 ⁵Forschungszentrum Jülich GmbH, IEK-7, Jülich, Germany

13 Corresponding author email: suvarna@tropmet.res.in

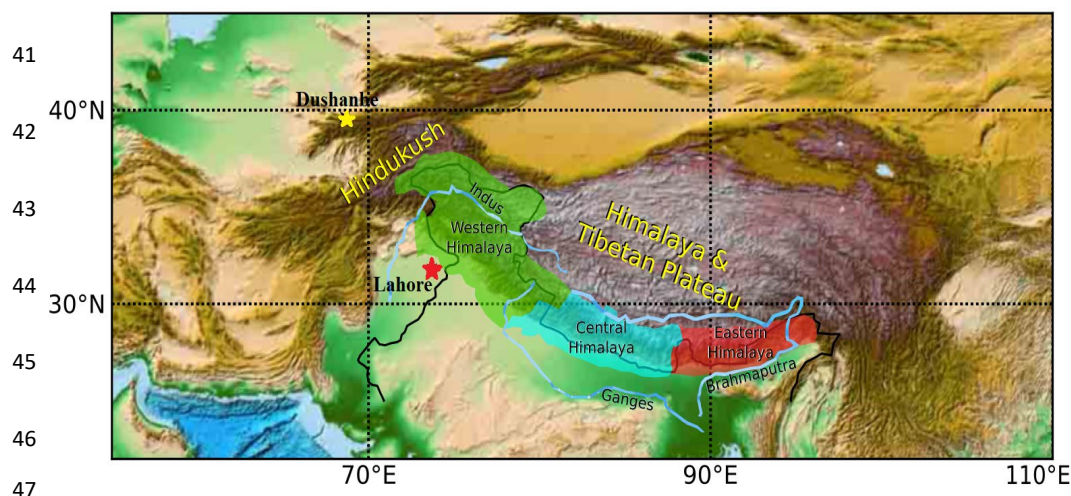
14 **Abstract**

15 The rapid melting of glaciers in the Hindu Kush Himalayas (HKH) during recent decades poses
16 an alarming threat to water security for larger parts of Asia. If this melting persists, the entire
17 Himalayan glaciers is estimated to disappear by end of 21st century. Here, we assess the
18 influence of the spring 2020 COVID-19 lockdown on the HKH, demonstrating the potential
19 benefits of a strict emission reduction roadmap. Chemistry-climate model simulations,
20 supported by satellite and ground measurements, show that lower air pollution during
21 lockdown led to a reduction in black carbon in snow (2-14%) and thus in snow melting
22 (10-40%). This caused increases in snow cover (6-12%) and mass (2-20%) and a decrease in
23 runoff (5-55%) over the HKH and Tibetan Plateau, ultimately leading to an enhanced snow-
24 water-equivalent (3.3–55%). We emphasize the necessity for immediate anthropogenic
25 pollution reductions to address the hydro-climatic threat to billions of people in South Asia.



126 **1. Introduction**

27 The Hindu Kush Himalayan (HKH) mountains and Tibetan plateau is the largest snow-cladded
28 region outside the Poles (Fig. 1). The HKH meltwater feeds rivers in India and China that drive
29 the agriculture, hydropower generation, and economy of these countries (Hussain et ., 2019,
30 Sabin et al., 2020, Lee et al., 2021a). The Himalayan snowmelt in spring provides ~50% of the
31 annual freshwater to ~4 billion people of South Asia and East Asia (sabin et al., 2020, Sarangi,
32 et al., 2019). Although snowmelt benefits freshwater supply to people, rapid Himalayan
33 snowmelt caused a loss of ~40 % of the Himalayan glacier area compared to the Little Ice Age,
34 400 to 700 years ago, i.e. ~0.92 to 1.38 mm sea-level equivalent (Lee et al., 2021b). The snow
35 mass over the Himalayas has generally decreased during the last 30 years (except for a few
36 Karakoram glaciers that show an increasing trend in snow mass). The alarming rate of snow
37 melting of 0.02 to 0.6 cm °C⁻¹ day⁻¹ raised concerns about the sustainability of water supply
38 and loss of glaciers in the region (Hussain et ., 2019, Lee et al., 2021b, Tiwari et al., 2015).
39 Model simulations for extreme scenarios show that Himalaya snow melting could cause the
40 glaciers to disappear by the end of the 21st century (Cruz et al., 2007, Hock et al., 2019).



48 **Figure 1:** Map of the Hindu Kush Himalayas region with the Western (70 - 80° E, 30° - 35° N),
49 Central (80° - 87° E, 28° - 30° N), and Eastern Himalayas (88° - 95° E, 26° - 30° N). A yellow



50 and red star indicates the location of the AERONET sun photometer stations Dushanbe
51 (68.858° E, 38.553 ° N) and Lahore (74.264° E, 31.480° N), respectively.

52 The accelerated thinning of Himalayan glaciers is attributed to climate change causing
53 shifts in air temperature and precipitation, as well as the atmospheric distribution and
54 deposition of light-absorbing particles i.e., dust, black carbon (BC) (IPCC 2013, Krishnan et
55 al., 2019). Among the aforementioned factors, snow darkening due to the deposition of
56 absorbing aerosols is an integral component of Himalayan snowmelt and runoff (Lau et al.,
57 2010). The snow-melting efficacy of BC is higher than that of greenhouse gases (Sarangi et al.,
58 2019, Qian, et al., 2011, Nair, et al., 2013, Ma et al., 2019). The increasing energy demand of
59 the densely populated South Asian region has increased the emission of greenhouse gases and
60 BC aerosol in the last few decades (Fadnavis et al., 2017, Krishnan et al., 2020), leading to
61 enhanced darkening and snow melting (Usha et al., 2021).

62

63 The economic slowdown caused by the COVID-19 pandemic measures led to a drastic
64 reduction in public and freight transportation, industrial emissions, and energy use (Fadnavis
65 et al., 2021). This resulted in a substantial decline in emissions of several atmospheric
66 pollutants including greenhouse gases and black carbon aerosol (Forster et al., 2020, Kanniah
67 et al., 2020, Le Quéré et al., 2020) and potentially reduced deposition of dark aerosols on snow
68 and ice (Bair et al., 2021). Remote sensing observations show cleaner snow with ~30% less
69 light-absorbing impurities in snow during the lockdown period over Asia between Mach and
70 May 2020 (Bair et al., 2021). This led to decreased snowmelt by 25 – 70 mm in 2020 compared
71 to the last 20-year mean over Western Himalayas due to decreased radiative forcing induced
72 by BC and dust deposition on snow/ice surfaces and related changes in in-snow absorption and
73 surface albedo (Bair et al., 2021). Impacts of reduced levels of air pollution on changes in the
74 snow mass, surface water runoff, and water reservoir over the HKH are not reported hitherto.



75 Here, we provide a detailed analysis of the impact of reduced pollution over HKH and Tibetan
76 plateau region during the COVID-19 lockdown period between March and May 2020. We used
77 global simulations with the chemistry-climate model ECHAM6-HAMMOZ (Tegen et al.,
78 20219, Schultz, et al., 2018) updated with an improved BC-in-snow parameterization, in order
79 to contrast the COVID-19 (COVID) with the typical, unchanged (control, CTL) air pollution
80 conditions. The COVID simulations are performed using a COVID-19 emission inventory
81 where emissions are reduced based on Google and Apple mobility data (Forster, et al., 2020)
82 (details in Appendix A).

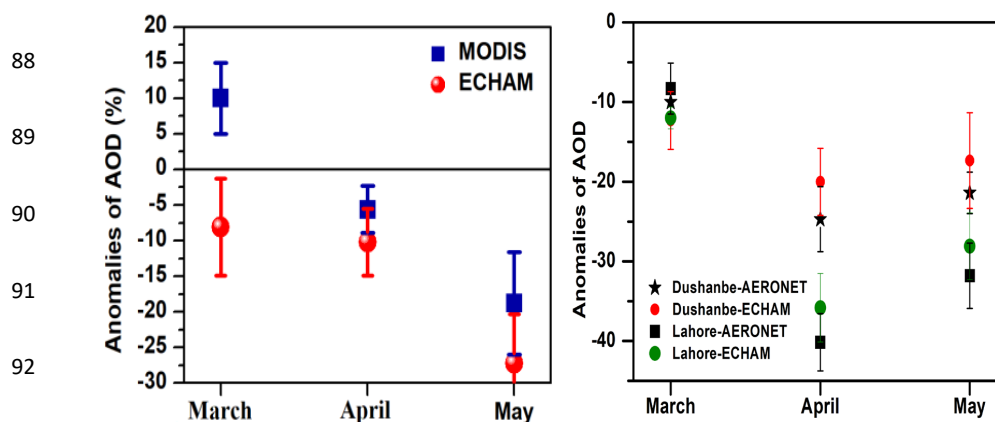
83

84 2. Results

85

86 2.1 Reduction of airborne aerosols and in-snow BC concentration over the Himalayas

87



88

89
90
91
92
93
94 **Figure 2:** (a) Changes in monthly mean AOD (%) during March - May 2020 from MODIS in
95 comparison to mean of 2001-2019 and ECHAM-HAMMOZ (COVID minus CTL) averaged
96 over the Hindu Kush Himalayas (HKH) and Tibetan Plateau region (75° - 95° E, 30° - 35° N),
97 (b) same as (a) but for AOD from AERONET observations and ECHAM-HAMMOZ model
98 results at Dushanbe (68.858° E, 38.553° N, climatology 2010-2019) and Lahore (74.264° E,



99 31.480° N, climatology 2006-2019). Vertical bars in Fig (a)-(b) indicate the standard deviation
100 within ten members of model simulations.

101

102 The COVID-19 lockdown restrictions in spring 2020 decreased the anthropogenic
103 aerosol amounts over the HKH ranges (Western, Central, and Eastern Himalayas), and the
104 Tibetan Plateau region. The ECHAM6-HAMMOZ model simulations show that COVID
105 lockdown resulted in a cleaner atmosphere during March - May 2020 over the HKH ranges and
106 Tibetan Plateau region. There is a reduced level of Aerosol Optical Depth (AOD) over the
107 region throughout spring 2020 by $-8.1\pm 6.2\%$ in March, $-10.2\pm 4.7\%$ in April, $-27\pm 6.9\%$ in
108 May compared to the CTL (non COVID) simulation (Fig. 2a). This is supported by NASA's
109 Moderate Resolution Imaging Spectroradiometer (MODIS) measurements also showing a
110 reduction in AOD in April ($-5.6\pm 3.3\%$) and May ($-18.8\pm 7.2\%$) 2020 compared to the mean
111 over the last 20 years (Fig 2a). Thus, both model simulations and MODIS AOD show a
112 reduction in aerosol pollution in April - May 2020. For March 2020, MODIS measurements
113 show AOD enhancement by $10.2 \pm 4.8\%$, which is due to increased dustiness over the HKH
114 region (see Appendix B for a detailed discussion). AOD measurements at two Aerosol Robotic
115 Network (AERONET) sun photometer stations in Dushanbe (68.858° E, 38.553° N),
116 and Lahore (74.264° E, 31.480° N) show an AOD reduction in agreement with our model
117 simulations (Fig. 2b). There are differences among MODIS, AERONET and the model. The
118 changes in AOD during COVID compared to no-COVID period is smaller in the model than
119 the MODIS observations by $4.2 - 9.8\%$ and larger than the AERONET observations by 1.8
120 $- 4.2\%$. These differences are due to the fact that the simulated AOD change is in response to
121 the reduction of anthropogenic aerosols and associated circulation responses, while MODIS
122 and AERONET measurements show the effect of all atmospheric processes. Also, note that the
123 MODIS AOD values are spatial averages representative for a relatively large area while the
124 AERONET values are point measurements. Importantly, changes in simulated AOD in 2020



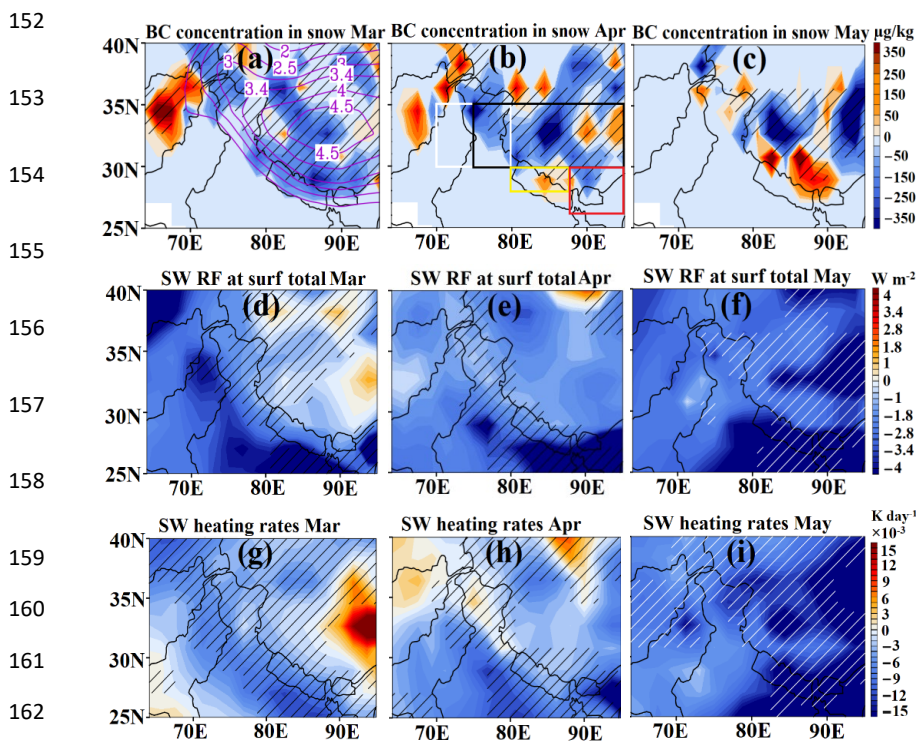
125 fall within the standard deviation of satellite and ground-based measurements indicating
126 reliability of our simulations (except for March 2020 with respect to MODIS). Our model
127 simulations also show a reduction in BC burden by 15 -55% (Fig. S1a), and sulfate burden by
128 22 - 24 % over the HKH and Tibetan Plateau regions in spring 2020 (Fig. S1b). Interestingly,
129 dust burden also shows a reduction over these regions (Fig. S1c and Fig. S2), except over
130 central Himalaya in March and April 2020 (details in Appendix B). A drop in BC is also
131 observed in Aerosol Radiative Forcing Over India Network (ARFINET) ground-based
132 measurements over the Indo-Gangetic Plain (> 50 %), north-eastern India (>30%), Himalaya
133 regions (16 - 60%), and Tibet (70%) during spring 2020 (Gogoi et al., 2020, Liu et al., 2020)
134 Similar impact of reduction of energy consumptions on decrease in AOD during the COVID-
135 19 lockdown period, i.e., in spring 2020 compared to the 2010-2019 climatology are also seen
136 over South and East Asia (40 %) and Indo-Gangetic Plain (IGP) by 30 – 40 % in satellite
137 measurements (Fadnavis et al., 2021, Srivastava et al., 2021, Pandey et al., 2021, Shafeeqe et
138 al., 2021).

139

140 The reduction in anthropogenic air pollution leads to a reduction in BC concentration
141 in the snow $\sim 25 - 350 \mu\text{g kg}^{-1}$ (by 12 – 35 %) during spring 2020 (Fig. 3a-c) that reduce the
142 snow darkening effect by embedded aerosol impurities. Our simulations reveal that the
143 decrease in BC concentration in the snow has decreased the shortwave radiative forcing at the
144 surface by $0.2 - 2 \text{ W m}^{-2}$ in March - May 2020 (Fig. 3 d-f), leading to a decrease in tropospheric
145 heating by solar radiation of 0.001 to 0.015 K day^{-1} (Fig. 3 g-i). The reduced BC in the
146 atmosphere over the HKH and Tibetan Plateau region resulted in less absorption and re-
147 emission of longwave radiation and, as a consequence, there is a reduction in longwave
148 radiative forcing in the atmosphere leading to a lower atmospheric heating (Fig. S3). Therefore,
149 the reduction of anthropogenic sulfate, and BC burden, combined with lower atmospheric



150 loadings of BC, PM_{2.5} and PM₁₀, as well as BC in snow resulted in decreased heating of the
 151 snowpack and tropospheric column.



164 **Figure 3:** Spatial distribution of anomalies (COVID minus CTL) of BC concentration in snow
 165 ($\mu\text{g kg}^{-1}$) for (a) March, (b) April, and (c) May 2020; (d-f) shortwave radiative forcing (W m^{-2})
 166 at the surface and (g-i) tropospheric heating rates (K day^{-1}) due to changes in BC
 167 concentration in snow (COVID minus CTL). Hatched areas indicate the 95%-significance
 168 level. Contours in panel (a) indicate topography in km. Boxes in panel (b) indicate boundaries
 169 of Western Himalayas (WH, white), Central Himalayas (CH, yellow), Eastern Himalayas (EH,
 170 red) and Tibetan Plateau (black).

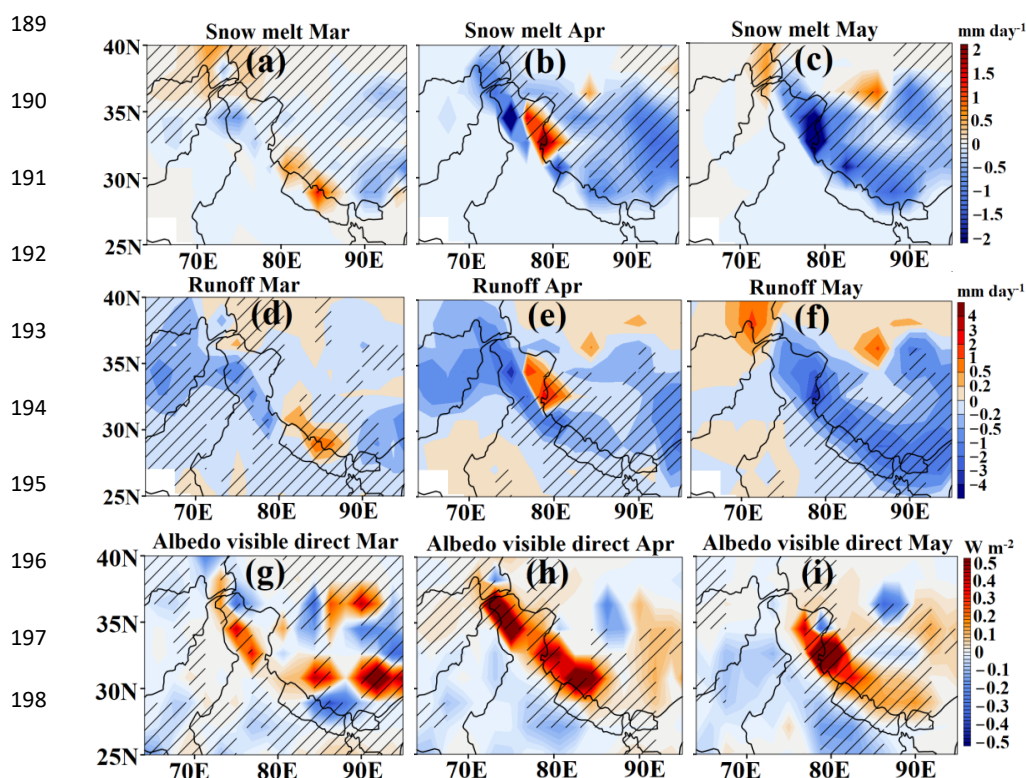
171

172 2.2 Impacts on snow melting, surface water runoff, and snow cover

173 Further we show that the decrease in aerosol pollution reduced the snow melting in
 174 spring 2020 by 0.2 to 2.5 mm day^{-1} corresponding to 10 – 50 % (Fig. 4 a-c). The amount of
 175 reduction of snow melting is pronounced over the western Himalayas in May. As a result of a



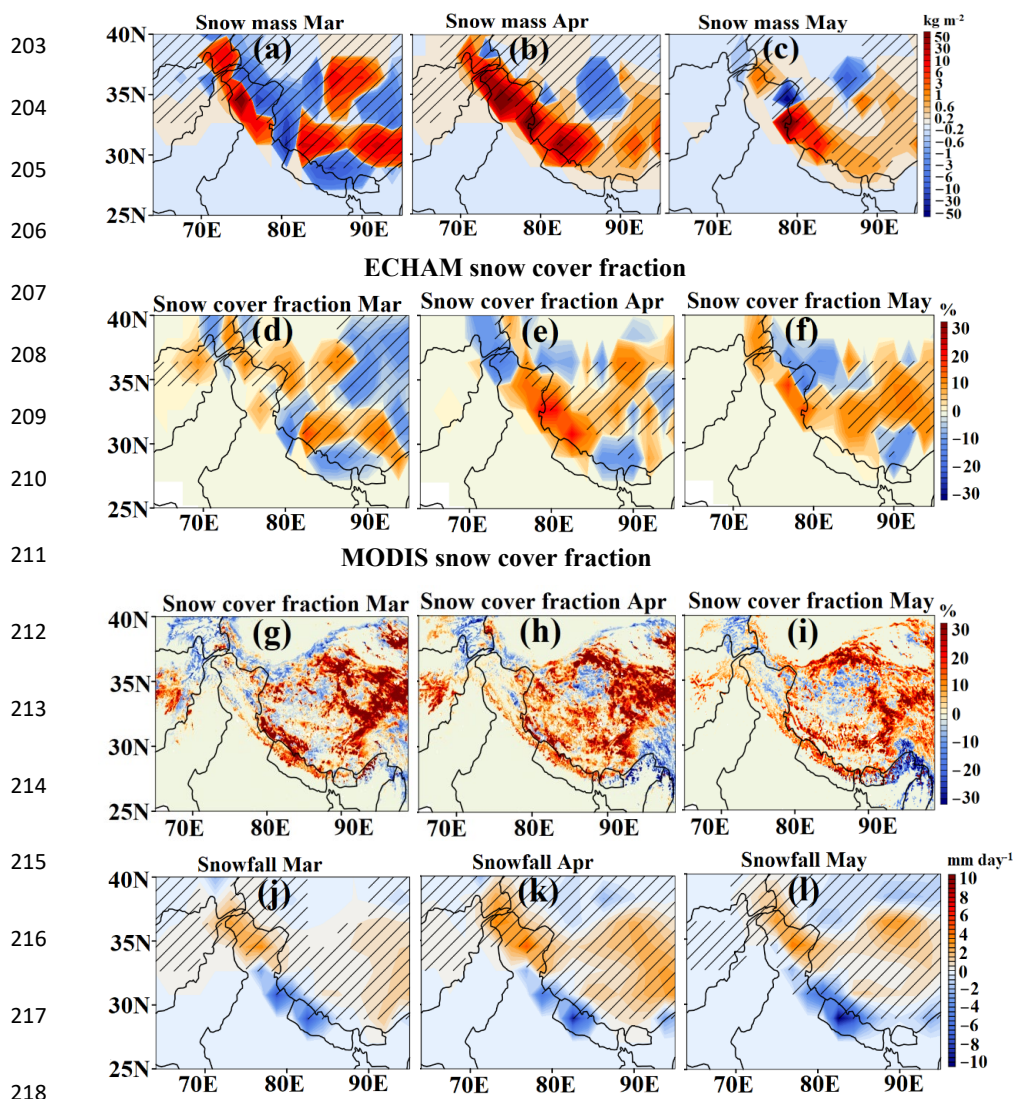
176 reduction in snowmelt, surface water runoff has been drastically reduced by 2-4 mm day⁻¹ (5 -
177 55 %) (Fig. 4 d-f). The reduction in the runoff is most pronounced in May over the entire
178 Himalayas and central Tibetan Plateau region. Estimates from remote sensing measurements
179 also show the reduction of runoff by 6.5 km³ of melted water in the Indus River Basin (Bair et
180 al., 2021). In the past, studies have shown that elevated levels of light-absorbing aerosols
181 (elemental carbon: 13 to 75 ng g⁻¹ and dust: 32 to 217 µg g⁻¹) can contribute to about 3 to
182 10 mm day⁻¹ of snowmelt over western Himalayas (Thind et al., 2019). Sensitivity analysis
183 using a glacier mass balance model shows that a BC-induced snow albedo reduction resulted
184 in an increase in runoff by 4 – 18% annually (Santra, et al., 2019). In contrast to impacts of
185 rising anthropogenic emissions during the past decades, emission reductions during the 2020
186 COVID-19 lockdown period caused a brighter albedo that led to an enhanced reflection of 0.2
187 - 0.5 W.m⁻² (see Fig. 4g-i), reducing atmospheric heating, snow melting and runoff in spring
188 2020.





199 **Figure 4:** Spatial distribution of anomalies of (a-c) snow melt (mm day^{-1}), (d-f) surface water
200 runoff (mm day^{-1}) for March to May 2020 (COVID minus CTL) and (g-i) surface albedo mean
201 in the visible (W m^{-2}). Hatched areas indicate the 95%-significance level.

202



219 **Figure 5:** Monthly mean anomalies (COVID minus CTL) of the (a-c) snow mass (kg m^{-2}), and
220 (d-f) snow cover fraction (%) for March to May 2020 as modelled by ECHAM6-HAMMOZ
221 as well as (g-i) snow cover fraction anomalies from MODIS satellite measurements (%) with
222 respect to the climatological average 2000-201, (j-l) monthly mean anomalies of the snowfall



223 for March to May 2020 as modelled by ECHAM6-HAMMOZ (COVID minus CTL). Hatched
224 areas indicate the 95%-significance level.

225

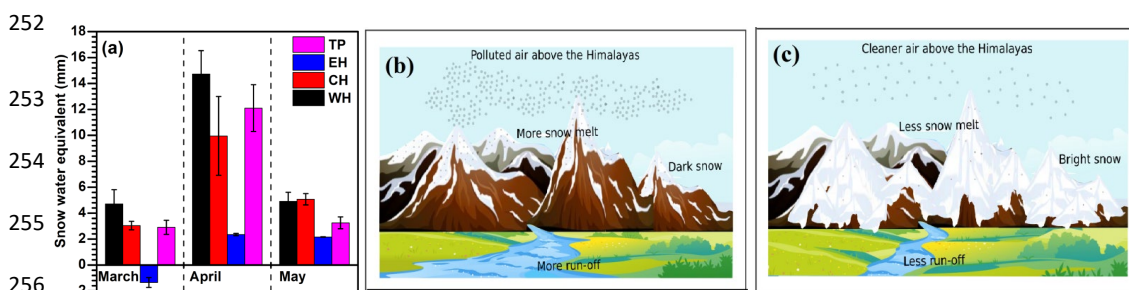
226 Our simulations also indicate that these changes lead to an increase in snow mass of
227 0.2-50 kg m⁻², i.e. 10-40% (Fig. 5a-c) and snow cover fraction of 2-30% during spring 2020
228 (Fig. 5d-f). MODIS measurements (Fig. 5g-i) also show a remarkable agreement with the
229 model simulations (especially during April - May 2020), with increased snow cover of about
230 15-30% over the parts of Western Himalayas and Central Himalayas and the Tibetan Plateau
231 region and decreased by 5-12 % over parts of North-East Himalayas especially in April and
232 May 2020. However, there are also some differences in terms of exact regions of snow cover
233 enhancement or reduction respectively, since the MODIS observations include the influence of
234 real-time meteorology, while meteorology in the model ensemble include internal variability.
235 Our model simulations show that pollution changes in COVID-19 lockdown period and
236 associated changes in meteorology has increased snowfall (2-5 mm day⁻¹, 3-20 %) over the
237 Western Himalayas and Tibetan Plateau region (Fig 5j-i). The increase in snowfall over these
238 regions will contribute to enhancement in snow mass and snow cover (Fig. 5 a-i) and albedo
239 (Fig. 4 g-i).

240

241 The impact of reduced pollution on the snow water in the Himalayas from our model
242 simulations is illustrated in Fig. 6a. The snow mass enhancement led to increase in the snow
243 water equivalent by 2.1 to 14.7 mm (3.3 to 55 %). The Western Himalayas show the highest
244 increase in snow water equivalent by 14.7 mm (55 %) followed by the Tibetan Plateau by 12
245 mm (by 22 %) and Central Himalayas by 10 mm (by 18%) in April. While the Eastern
246 Himalayas show a decrease in March (-1.3 mm; 10 %) and small enhancement in April by
247 2.1mm (3.3 %) and May 2020 by 2.3 mm (3.7%) due to pollution reduction. Thus, human
248 induced pollution reduction during the COVID-19 lockdown benefitted the HKH in many



249 ways. A schematic shows the COVID-19 lockdown-induced effects in Figs. 6b-c: increased
250 snow surface reflectivity, reduced snowmelt and surface water runoff, as well as enhanced
251 snow water.



257 **Figure 6:** (a) Anomalies (CTL minus COVID) in snow water equivalent (mm) from March to
258 May 2020 over the Western Himalayas (WH), Central Himalayas (CH), Eastern Himalayas
259 (EH) and Tibetan Plateau (TP). Vertical bars indicate the standard deviation within ten
260 members of model simulations. Schematic illustrating the impacts of (b) air pollution on snow
261 darkening in the Himalayas and surface water runoff than for usual polluted case and (c) the
262 impacts of reduced pollution on snow brightening in the Himalayas and reduced surface water
263 runoff, as observed during the 2020 COVID-19 lockdown period.

264

265 **3. Summary and conclusions:** A rising trend in Asian air pollution and
266 associated climate change over the last few decades have had a detrimental impact on snow
267 melting over the Hindu Kush Himalayas (HKH) and Tibetan Plateau region³². Black carbon
268 from increasing emissions of biomass burning, industrial and domestic combustion and
269 transport is deposited on snow, reducing its albedo (i.e. darkening). A snow darkening effect,
270 compounded with other climate change effects, accelerates the melting of snow and the
271 disappearance of ice cover over the HKH and Tibetan Plateau region at an extraordinary rate
272 (Usha et al., 2021). The drop in anthropogenic air pollution emissions, e.g. from energy
273 production, during the COVID-19 lockdown period in spring 2020 reduced air pollutant levels
274 worldwide (Forster, et al., 2020). Our model simulations indicate that the associated reduction
275 in anthropogenic aerosols and greenhouse gases in spring 2020 have benefited the HKH. It



276 caused an enhancement in the snow cover fraction by 6 - 12 % and snow mass by 2 - 20 %,
277 corresponding to a decrease in snow melting by 10 – 40 % and surface water runoff by 0.2 - 3
278 mm day⁻¹. As a consequence, the amount of snow water equivalent is increased considerably
279 by 3.3 to 55 %.

280 Our findings highlight that out of the two processes causing a retreat of Himalayan
281 glaciers: (1) a slow response to global climate change and (2) a fast response to local air
282 pollution (especially black carbon), a policy action on the latter is more likely to be within
283 reach of possible policy action on a shorter-term time scale. Even if we stopped CO₂ emissions
284 immediately, temperatures would not start decreasing. Our findings confirm the importance of
285 reducing short-lived climate forcers (Black carbon) and their complementary role to CO₂
286 mitigation (Rogelj et al., 2014). Reduction of air pollution to levels similar with those recorded
287 during the 2020 COVID-19 lockdown period, could safeguard HKH glaciers, which are
288 otherwise under the threat to disappear by 21st century. Since 2000 Himalayan glaciers have
289 been losing nearly half a meter of ice a year (Wester et al., 2019). Our estimates indicate that
290 air pollution reduction during COVID 19 lockdown in spring 2020 caused reduction in snow
291 melt by 0.5 to 1.5 mm day⁻¹, indicating large benefits to HKH glaciers. Even if global warming
292 is kept below 1.5°C, one third of the glaciers in the HKH region and more than half of those in
293 the Eastern Himalaya will likely be lost by the end of this century (Bolch et al., 2019). The
294 speedily retreating glaciers and the snowpack loss are already posing a threat to domestic
295 sustainable water resources for billions of people in Asia (Wood et al., 2020). However, if new
296 economically and technically feasible policies would reduce emissions of air pollutants (in
297 particular black carbon) to at least lockdown period levels, snowmelt could be reduced by 10
298 – 50%. Such policies will therefore bring substantial benefits for sustained water supply,
299 agriculture, and ecosystems in large parts of Asia.



300 **Appendix A: Methods:**

301 **A1.1 Observational data**

302 We used monthly snow cover fraction from NASA's Moderate Resolution Imaging
303 Spectroradiometer (MODIS) satellite product on a $0.5 \times 0.5^\circ$ resolution (version 6, level 3) (Hall
304 et al., 2006) for the years 2000 – 2020 (<https://nsidc.org/data/MOD10CM/versions/6>). For
305 aerosol information we used monthly mean satellite AOD at $1 \times 1^\circ$ resolution from the MODIS
306 Terra level-3 dark target and deep blue retrievals at 550 nm wavelength for 2001-2020
307 (<https://giovanni.gsfc.nasa.gov>). We also used ground-based sun photometer observations of
308 AOD from the Aerosol Robotic Network (AERONET) (Martonchik et al., 2004) at the stations
309 Dushanbe (68.858° E, 38.553° N) for the period 2010-2020 and Lahore (74.264° E, 31.480° N)
310 for the period 2006 – 2020, situated in HKH region (<https://aeronet.gsfc.nasa.gov>).

311

312 **A1.2 The ECHAM6-HAMMOZ model description and Experimental set-up**

313 We performed 10-member ensemble experiments using the state-of-the-art aerosol-
314 chemistry-climate model ECHAM6-HAMMOZ (version echam6.3-ham2.3-moz1.0 (Schultz,
315 et al., 2018, Tegan et al., 2019). The model comprises the atmospheric general circulation
316 model ECHAM6 (Stevens et al., 2013), the tropospheric chemistry module (Schultz, et al.,
317 2018), and the Hamburg Aerosol Model (HAM) (Stier et al., 2005, Zhang et al., 2012). The
318 HAM component predicts the nucleation, growth, evolution, and sinks of sulphate (SO_4^{2-}),
319 black carbon (BC), organic carbon (OC), sea salt (SS), and mineral dust (DU) aerosols. Seven
320 log-normal modes describe the size distribution of the aerosol population with a prescribed
321 variance in the aerosol module. The MOZ submodule describes the trace gas chemistry from
322 the troposphere to the lower thermosphere. The chemical mechanism includes the O_x , NO_x ,
323 HO_x , ClO_x and BrO_x chemical families, along with CH_4 and its degradation products. Several



324 primary non-methane hydrocarbons (NMHCs) and related oxygenated organic compounds are
325 also described. It contains 108 species, 71 photolytic processes, 218 gas-phase reactions and
326 18 heterogeneous reactions with aerosol (Schultz, et al., 2018). Details of emissions
327 (anthropogenic, biomass burning, biogenic, fossil fuel etc.) and model parametrisation and
328 other details are reported in the past (Fadnavis, et al., 2017, 2019,a,b 2021). Anthropogenic and
329 biomass burning emissions of sulphate, and black carbon (BC) and organic carbon (OC) are
330 based on the AEROCOM-ACCMIP-II emission inventory for year 2020 (Lamarque et al.,
331 2010, Textor et al., 2006). Additional consideration for the reduction of snow albedo due to
332 BC in snow is implemented but extended for the MOZ module (Huang, 2018). Snow albedo
333 reduction is calculated by considering the concentration of BC in the top layer of surface snow.
334 Influxes of BC in snow include below-cloud and in-cloud wet scavenging, as well as dry
335 deposition and sedimentation. Snowmelt and glacier runoff remove the in-snow BC at a
336 reduced efficiency, leading to enhanced concentration, while fresh and pristine snowfall leads
337 to reductions in BC concentration.

338

339 The model simulations were performed at T63 horizontal resolution ($1.875^{\circ} \times 1.875^{\circ}$) with 47
340 levels in the vertical from the surface to 0.01 hPa (corresponding to approx. 80 km), and with
341 a time step of 20 minutes. To understand the effect of the COVID-19 restrictions on snow over
342 Himalayas and Tibetan plateau region we conducted a control (CTL) and a COVID-19
343 (COVID) simulation. We adopted an ensemble approach (with 10 ensemble members) for the
344 above two experiments. Ten spin-up simulations were performed from 1 to 31 December 2019
345 to generate stabilised initial fields for the 10 ensemble members. Emissions were the same in
346 each of the 10 members during the spin-up period. Control simulations were extended with the
347 same setup until 1 July 2020. While for the COVID simulations (10 ensemble members each),
348 the anthropogenic emission of all gases and aerosols were changed since 1 January 2020



349 according to Google and Apple mobility data (Forster et al., 2020). The COVID-19 emissions
350 were prepared by deriving scaling factors between the input4MIPS SSP245 baseline and the
351 version5, 2-year blip scenario (Forster et al., 2010), separately for each species and each grid
352 point (see Fig. S4a). Subsequently, these scaling factors have been applied to the AeroCom-II
353 ACCMIP emissions. This ensures consistency of the drop in emissions independent of the
354 absolute emission values in the AeroCom-II ACCMIP and the input4MIPS SSP245 data sets.
355 The global mean emission changes in carbon monoxide (CO, 2-24%), black carbon (BC, 3-
356 23%), organic carbon (OC, 2-17%), sulfur dioxide (SO₂, 3-23%), nitrogen oxides (NO_x, 2-
357 30%), methane (CH₄, 2-5%), and ammonia (NH₃, 0-3%) during the period January to 1 July
358 2020 (COVID - CTL) are in agreement with previous studies (Foster et al., 2020, Le Quéré et
359 al., 2020) (Fig. S4b). The COVID and CTL simulations ended on 1 July 2020. To investigate
360 the effects of COVID-19 emissions in spring (i.e., since 1 March 2020), we analysed the
361 difference between COVID and CTL simulations for the spring season in 2020. The same dust
362 parametrisation was employed in the CTL and COVID simulations.

363

364 **Appendix B: Comparison of AOD over Western, Central, Eastern Himalayas and** 365 **Tibetan Plateau regions**

366 We elaborate on the comparison of MODIS AOD with our model simulations over
367 Western, Central, Eastern Himalayas and Tibetan Plateau regions (Fig. S5). Both MODIS and
368 the model show a reduction in AOD during spring 2020 over the aforementioned regions of
369 HKH. The estimated differences in AOD during March to May 2020 vary between 0.8 – 11%
370 over Western and Central Himalayas, and 8 – 16% over Eastern Himalayas. Over the Tibetan
371 plateau region, in contrast to the model simulations, MODIS shows an enhancement (2 – 16 %)
372 in AOD (Fig. S5). This may be due to dust aerosols, which are transported during spring from



373 western Asia and locally, generating dust piles over the Tibetan Plateau (adnavis et al., 2017,
374 2021). The simulated dust aerosol concentration in spring 2020 over the Tibetan Plateau region
375 is smaller than no COVID situation (Fig. S1c, Fig. S2). The simulated dust is a response to
376 meteorology difference between the COVID and CTL simulations (Fig. S6).



377 References:

- 378 Bair, E., Stillinger, T., Rittger, K. & Skiles, M. COVID-19 lockdowns show reduced pollution
379 on snow and ice in the Indus River Basin. *Proc. Natl. Acad. Sci. U. S. A.* 118, 19–21,
380 <https://doi.org/10.1073/pnas.2101174118>, 2021.
- 381 Bolch, T. *et al.* Status and Change of the Cryosphere in the Extended Hindu Kush Himalaya
382 Region. in *The Hindu Kush Himalaya Assessment: Mountains, Climate Change,*
383 *Sustainability and People* (eds. Wester, P., Mishra, A., Mukherji, A. & Shrestha, A. B.)
384 209–255 (Springer International Publishing). doi:10.1007/978-3-319-92288-1_7 2019,
385 2019.
- 386 Cruz, R.V., Harasawa, H., Lal, M., Wu, S, Anokhin, Y., Punsalmaa, B., Honda, Y., Jafari, M.,
387 Li, C., and Huu Ninh, N. Climate change 2001: impacts, adaptation, and vulnerability.
388 *Choice Rev. Online* 39, 39-3433-39–3433, 2007.
- 389 Fadnavis, S., Kalita, G., Ravi Kumar, K., Gasparini, B. & Li, J. L. F. Potential impact of
390 carbonaceous aerosol on the upper troposphere and lower stratosphere (UTLS) and
391 precipitation during Asian summer monsoon in a global model simulation. *Atmos. Chem.*
392 *Phys.* 17, 11637–11654, <https://doi.org/10.5194/acp-17-11637-2017>, 2017.
- 393 Fadnavis, S., Sabin T. P, Rap A., Müller R., Kubin A. and Heinold B., The impact of COVID-
394 19 lockdown measures on the Indian summer monsoon. *Environ. Res. Lett.* 16, DOI
395 10.1088/1748-9326/ac109c, 2021.
- 396 Fadnavis, S. Müller R., Chakraborty T., Sabin T. P., Laakso A., Rap A., Griessbach S., Vernier
397 J-P. & Tilmes S. The role of tropical volcanic eruptions in exacerbating Indian droughts.
398 *Sci. Rep.* 11, 1–13, <https://doi.org/10.1038/s41598-021-81566-0>, 2021.
- 399 Fadnavis, S. Müller R., Kalita G, Rowlinson M., Rap A., Frank Li J-L, Gasparini B, and
400 Laakso A. The impact of recent changes in Asian anthropogenic emissions of SO₂ on sulfate
401 loading in the upper troposphere and lower stratosphere and the associated radiative
402 changes.. *Atmos. Chem. Phys.* 1–44, <https://doi.org/10.5194/acp-19-9989-2019>, 2019a.
- 403 Fadnavis, S. Sabin T. P., Roy C., Rowlinson M, Rap A, Vernier J-P. & E. Sioris C. E.. Elevated
404 aerosol layer over South Asia worsens the Indian droughts. *Sci. Rep.* 9, 1–12,
405 <https://doi.org/10.1038/s41598-019-46704-9>, 2019b.
- 406 Forster, P. M. *et al.* Current and future global climate impacts resulting from COVID-19. *Nat.*



- 407 *Clim. Chang.* 10, 913–919, 2020.
- 408 Gogoi, M. M. S. Babu S., Arun B. S., Krishna, Moorthy K., Ajay A., Ajay P., Suryavanshi A.,
409 Borgohain A., *et al.* Response of Ambient BC Concentration Across the Indian Region to
410 the Nation-Wide Lockdown: Results from the ARFINET Measurements of ISRO-GBP.
411 *Curr. Sci.* 120, 341, doi: 10.18520/cs/v120/i2/341-351, 2021.
- 412 Hall, D. K. MODIS / Terra Snow Cover 5-Min L2 Swath 500m. *Color. USA NASA Natl. Snow*
413 *Ice Data Cent. Distrib. Act. Arch. Cent* 5, 2006.
- 414 Huang, W. T. K. Aerosol effects on climate, with an emphasis on the Arctic.
415 <https://doi.org/10.3929/ethz-b-000319114> 2018, 2018
- 416 Hussain, A. Sarangi G.K., Pandit A., Ishaq S., Mammun N., Ahmad B., Jamil M.K., Hydropower
417 development in the Hindu Kush Himalayan region: Issues, policies and opportunities.
418 *Renew. Sustain. Energy Rev.* 107, 446–461, <https://doi.org/10.1016/j.rser.2019.03.010>,
419 2019.
- 420 Hock, R. *et al.* Chapter 2: High Mountain Areas. IPCC Special Report on the Ocean and
421 Cryosphere in a Changing Climate. *IPCC Spec. Rep. Ocean Cryosph. a Chang. Clim.* 131–
422 202, 2019.
- 423 IPCC Working Group 1, I. *et al.* IPCC, 2013: Climate Change 2013: The Physical Science
424 Basis. Contribution of Working Group I to the Fifth Assessment Report of the
425 Intergovernmental Panel on Climate Change. *Ippc AR5*, 1535, 2013.
- 426 Lamarque J.-F. , Bond T. C., Eyring V., Granier C., Heil A., Klimont Z., Lee D., Liousse
427 C., Mieville A., Owen B., Schultz M. G., Shindell D., Smith S. J., Stehfest E., Aardenne
428 J. Van, Cooper O. R., Kainuma M., Mahowald N., McConnell J. R., Naik V., Riahi K.,
429 and Vuuren D. P. van, Historical (1850-2000) gridded anthropogenic and biomass burning
430 emissions of reactive gases and aerosols: Methodology and application. *Atmos. Chem.*
431 *Phys.* 10, 7017–7039, <https://doi.org/10.5194/acp-10-7017-2010>, 2010.
- 432 Kanniah, K. D., Kamarul Zaman, N. A. F., Kaskaoutis, D. G. & Latif, M. T. COVID-19’s
433 impact on the atmospheric environment in the Southeast Asia region. *Sci. Total Environ.*
434 736, 139658, <https://doi.org/10.1016/j.scitotenv.2020.1396580048-9697>, 2020.
- 435 Krishnan, R., Shrestha, A., Ren, G., Rajbhandari, R., Saeed, S., & Sanjay, J. Unravelling
436 Climate Change in the Hindu Kush Himalaya: Rapid Warming in the Mountains and
437 Increasing Extremes. *The Hindu Kush Himalaya Assessment* (Springer Singapore).



- 438 doi:10.1007/978-3-319-92288-1_3, 2019.1
- 439 Krishnan, R. *et al.* Assessment of climate change over the Indian region: A report of the
440 ministry of earth sciences (MOES), government of India. Assessment of Climate Change
441 over the Indian Region: A Report of the Ministry of Earth Sciences (MoES), Government
442 of India (Springer Singapore). doi:10.1007/978-981-15-4327-2, 2020.
- 443 Lau, W. K. M., Kim, M. K., Kim, K. M. & Lee, W. S. Enhanced surface warming and
444 accelerated snow melt in the Himalayas and Tibetan Plateau induced by absorbing aerosols.
445 *Environ. Res. Lett.* 5, doi:10.1088/1748-9326/5/2/025204, 2010.
- 446 Lee, S. S., Chu, J. E., Timmermann, A., Chung, E. S. & Lee, J. Y. East Asian climate response
447 to COVID-19 lockdown measures in China. *Sci. Rep.* 11, 1–9, 2021a.
- 448 Lee, E., Carrivickl J. L., Quincey D. J., Cook S. J., Amesl W. H. M., & Brown L. E.,
449 Accelerated mass loss of Himalayan glaciers since the Little Ice Age. *Sci. Rep.* 11, 1–8,
450 <https://doi.org/10.1038/s41598-021-03805-8>, 2021b.
- 451 Le Quéré, C. Jackson R. B., M Jones M. W., Smith A. J. P., Abernethy S. Andrew R. M. , De-
452 Gol A. J. Willi D. R., Shan Y., Canadell J. G., Friedlingstein P., Creutzig F. and Peters G.
453 P., Temporary reduction in daily global CO₂ emissions during the COVID-19 forced
454 confinement. *Nat. Clim. Chang.* 10, 647–653, <https://doi.org/10.1038/s41558-020-0797-x>,
455 2020.
- 456 Liu, Y. Wang Y. , Cao Y., Yang Xi, T Zhang T., Luan M., Lyu D., Hansen A. D. A., Liu B., and
457 Zheng M., Impacts of COVID-19 on Black Carbon in Two Representative Regions in
458 China: Insights Based on Online Measurement in Beijing and Tibet. *Geophys. Res. Lett.*
459 48, 1–11, 10.1029/2021GL092770, 2021.
- 460 Ma, J. Zhang T., and GUAN X., The dominant role of snow/ice Albedo feedback strengthened
461 by black carbon in the enhanced warming over the Himalayas. *J. Clim.* 32, 5883–5899,
462 <https://doi.org/10.1175/JCLI-D-18-0720.s1.2019>.
- 463 Martonchik, J. V., Diner, D. J., Kahn, R., Gaitley, B. & Holben, B. N. Comparison of MISR
464 and AERONET aerosol optical depths over desert sites. *Geophys. Res. Lett.* 31, 1–
465 4, <https://doi.org/10.1029/2004GL019807>, 2004. \
- 466 Nair, V. S. Babu S. S., Moorthy K. K., Sharma A. K. , Marinoni A. & Ajai, Black carbon aerosols
467 over the Himalayas: Direct and surface albedo forcing. *Tellus, Ser. B Chem. Phys.*



- 468 *Meteorol.* 65, DOI: 10.3402/tellusb.v65i0.19738, 2013.\
- 469 Pandey, S. K. & Vinoj, V. Surprising changes in aerosol loading over india amid covid-19
470 lockdown. *Aerosol Air Qual. Res.* 21, 1–12, <https://doi.org/10.4209/aaqr.2020.07.0466>,
471 2021.
- 472 Qian, Y., Flanner, M. G., Leung, L. R. & Wang, W. Sensitivity studies on the impacts of Tibetan
473 Plateau snowpack pollution on the Asian hydrological cycle and monsoon climate. *Atmos.*
474 *Chem. Phys.* 11, 1929–1948, doi:10.5194/acp-11-1929-2011, 2011. Sabin, T., Krishnan,
475 R., Vellore, R., Priya, P., Borgaonkar, H., Singh, B., Sagar, A. Droughts and floods.
476 Climate Change Over the Himalayas. Assessment Of Climate Change Over The Indian
477 Region. doi:10.1007/978-981-15-4327-2_11, 2020.
- 478 Rogelj, J. Schaefferc M., Meinshausene M., Shindell D. T, Harec W., Klimontb Z. , Veldersh
479 G. J. M., Amannb M., and Schellnhuberr H.J., Disentangling the effects of CO2 and short-
480 lived climate forcer mitigation. *Proc. Natl. Acad. Sci. U. S. A.* 111, 16325–16330,
481 <https://doi.org/10.1073/pnas.1415631111>, 2014.
- 482 Santra, S. Verma1 S., Fujita K, Chakraborty I, Boucher O., Takemura T., Burkhardt John F.,
483 Matt F, and Sharma M., Simulations of black carbon (BC) aerosol impact over Hindu Kush
484 Himalayan sites: Validation, sources, and implications on glacier runoff. *Atmos. Chem.*
485 *Phys.* 19, 2441–2460, <https://doi.org/10.5194/acp-19-2441-2019>, 2019.
- 486 Sarangi, C. Qian Y., Rittger K., Bormann K.J., Liu Y., Wang H., Wan H., Lin G., and Painter
487 T.H., Impact of light-absorbing particles on snow albedo darkening and associated
488 radiative forcing over high-mountain Asia: high-resolution WRF-Chem modeling and new
489 satellite observations. *Atmos. Chem. Phys.* 19, 7105–7128, <https://doi.org/10.5194/acp-19-7105-2019>, 2019.
- 491 Schultz, M. G., Stadtler S., Schröder S., Taraborrelli D., Franco B., Krefting J, Henrot A. et
492 al., The chemistry-climate model ECHAM6.3-HAM2.3-MOZ1.0. *Geosci. Model Dev.* 11,
493 1695–1723, <https://doi.org/10.5194/gmd-11-1695-2018>, 2018.
- 494 Shafeeque, M. Arshad A., A Elbeltagi A., Sarwar A., Pham Q. B., S Khan S. N., I Dilawar A.
495 & Al-Ansari N., Understanding temporary reduction in atmospheric pollution and its
496 impacts on coastal aquatic system during COVID-19 lockdown: a case study of South Asia.
497 *Geomatics, Nat. Hazards Risk* 12, 560–580,
498 <https://doi.org/10.1080/19475705.2021.1885503>, 2021.



- 499 Srivastava, A. K., Bhojar P.D., Kanawade V. P., Devara P.C. S., Thomas A., Soni V.K.,
500 Improved air quality during COVID-19 at an urban megacity over the Indo-Gangetic Basin:
501 From stringent to relaxed lockdown phases. *Urban Clim.* 36, 100791,
502 <https://doi.org/10.1016/j.uclim.2021.100791>, 2021.
- 503 Stevens, B., Giorgetta M., Esch M., Mauritsen T., Crueger T., Rast S., Salzmann M., Schmidt
504 H., Bader J., Block K., Brokopf R., Fast I., Kinne S., Kornblueh L., Lohmann U., Pincus
505 R., Reichler T., Roeckner E. Atmospheric component of the MPI-M earth system model:
506 ECHAM6. *J. Adv. Model. Earth Syst.* 5, 146–172, <https://doi.org/10.1002/jame.20015>,
507 2013.
- 508 Stier, P., Feichter J., Kinne S., Kloster S., Vignati E., Wilson J., Ganzeveld L., Tegen
509 I., Werner M., Balkanski Y. Schulz M., Boucher O., Minikin A., and Petzold A., The
510 aerosol-climate model ECHAM5-HAM. *Atmos. Chem. Phys.* 5, 1125–1156,
511 <https://doi.org/10.5194/acp-5-1125-2005>, 2005.
- 512 Tegen, I., Neubauer D., Ferrachat S., Siegenthaler-Le Drian C, Bey, I., Schutgens N., Stier P.,
513 Watson-Parris D., et al., The global aerosol-climate model echam6.3-ham2.3 -Part 1:
514 Aerosol evaluation. *Geosci. Model Dev.* 12, 1643–1677, [https://doi.org/10.5194/gmd-12-](https://doi.org/10.5194/gmd-12-1643-2019)
515 1643-2019, 2019.
- 516 Thind, P. S., Chandel, K. K., Sharma, S. K., Mandal, T. K. & John, S. Light-absorbing
517 impurities in snow of the Indian Western Himalayas: impact on snow albedo, radiative
518 forcing, and enhanced melting. *Environ. Sci. Pollut. Res.* 26, 7566–7578,
519 <https://doi.org/10.1007/s11356-019-04183-5>, 2019.
- 520 Textor, Schulz M, Guibert S., Kinne S., Balkanski Y., Bauer S., Bernsten T., Berglen
521 T., Boucher O., Chin M., Dentener F, Diehl¹ T., Easter R., Feichter H., Fillmore
522 D., Ghan S., Ginoux P., Gong S., Grini A., Hendricks J. , Horowitz L., Huang
523 P., Isaksen I., Iversen I, Kloster S., Koch D., Kirkevåg A., Kristjansson J. E., Krol M.
524 , Lauer A., Lamarque J. F., Liu X., Montanaro V., Myhre G., Penner J., Pitari
525 G., Reddy⁵ S., Seland Ø., Stier P., Takemura T., and Tie X., Analysis and quantification
526 of the diversities of aerosol life cycles within AeroCom. *Atmos. Chem. Phys.* 6, 1777–1813,
527 <https://doi.org/10.5194/acp-6-1777-2006>, 2006.
- 528 Tiwari, S., Kar, S. C. & Bhatla, R. Snowfall and Snowmelt Variability over Himalayan Region
529 in Inter-annual Timescale. *Aquat. Procedia* 4, 942–949,doi: 10.1016/j.aqpro.2015.02.118,



- 530 2015.
- 531 Usha, K. H., Nair, V. S. & Babu, S. S. Effect of aerosol-induced snow darkening on the direct
532 radiative effect of aerosols over the Himalayan region. *Environ. Res. Lett.* 16,
533 <https://doi.org/10.1088/1748-9326/abf190>, 2021.
- 534 Wester P., Mishra A., Mukherji A., S. A. B. The Hindu Kush Himalaya Assessment—
535 Mountains, Climate Change, Sustainability and People. Springer Nature Switzerland AG,
536 Cham. doi:<https://doi.org/10.1007/978-3-319-92288-1>, 2019.
- 537 Wood, L. R. Neumann K., Nicholson K.N., Bird B.W., Dowling C. B. and Sharma S. Melting
538 Himalayan Glaciers Threaten Domestic Water Resources in the Mount Everest Region,
539 Nepal. *Front. Earth Sci.* 8, 1–8, <https://doi.org/10.3389/feart.2020.00128>, 2020.
- 540 Zhang, K. O'Donnell D., Kazil J., Stier P., Kinne S., Lohmann U., Ferrachat S., Croft B.,
541 Quaas J, Wan H., Rast S., and Feichter J., The global aerosol-climate model ECHAM-
542 HAM, version 2: Sensitivity to improvements in process representations. *Atmos. Chem.*
543 *Phys.* 12, 8911–8949, <https://doi.org/10.5194/acp-12-8911-2012>, 2012.

544

545 **Acknowledgments**

546 The authors thank the staff of the High Power Computing Centre (HPC) in IITM, Pune, India,
547 for providing computer resources and the team members of MODIS for providing data. We
548 thank Sabur F. Abdullaev and Brent Holben for their efforts in establishing and maintaining
549 Dushanbe and Lahore AERONET sites respectively.

550 **Author Contributions**

551 S.F. initiated the idea of the study. S.F., B. H. and K. H. designed and performed model
552 simulations. K. H. included a 'BC in snow' scheme in the ECHAM6-HAMMOZ model. A.R.
553 and A. K. prepared Google based emission inventory. T.P.S., R.M. performed data analysis
554 and contributed in overall design. All authors contributed to discussions of the results and the
555 writing of the manuscript.



556 **Data and code availability**

557 The ECHAM-HAMMOZ model source code and all required input data are available to the
558 scientific community according to the HAMMOZ Software License Agreement through the
559 project website: <https://redmine.hammoz.ethz.ch/projects/hammoz>. The data that support the
560 findings of this study are openly available in zenodo at DOI 10.5281/zenodo.6783077

561

562 **Competing Interests:** The authors declare no competing interests.

563

564